Antiangiogenic and anti-invasive effects of sunitinib on experimental human glioblastoma

Sophie de Boüard, Paulette Herlin, James G. Christensen, Edwige Lemoisson, Pascal Gauduchon, Eric Raymond, and Jean-Sébastien Guillamo

GRECAN, Centre François Baclesse, Université de Caen Basse-Normandie, 14076 Caen, France (S.D.B., P.H., E.L., P.G., J.-S.G.); Pfizer Inc., San Diego, CA 92121 USA (J.G.C.); Hôpital Beaujon, 92118 Clichy, France (E.R.); CHU Côte de Nacre, Département de Neurologie, 14033 Caen, France (J.-S.G.)

Angiogenesis inhibitors appear to be promising therapies for highly vascularized tumors such as glioblastoma multiforme (GBM). Sunitinib is an oral multitargeted tyrosine kinase inhibitor with both antiangiogenic and antitumor activities due to selective inhibition of various receptor tyrosine kinases, including those important for angiogenesis (vascular endothelial growth factor receptors and platelet-derived growth factor receptors). Here we evaluated the antitumor activities of sunitinib on orthotopic models of GBM in vitro and in vivo. Sunitinib potently inhibited angiogenesis that was stimulated by implantation of U87MG and GL15 cells into organotypic brain slices at concentrations as low as 10 nM. At high dose (10 μM), sunitinib induced direct antiproliferative and proapoptotic effects on GL15 cells and decreased invasion of these cells implanted into brain slices by 49% ($p < 0.001$). Treatment was associated with decreases in Src (35%) and focal adhesion kinase (44%) phosphorylation. However, anti-invasive activity was not observed in vivo at the highest dose level utilized (80 mg/kg per day). Survival experiments involving athymic mice bearing intracerebral U87MG GBM demonstrated that oral administration of 80 mg/kg sunitinib (five days on, two days off) improved median survival by 36% ($p < 0.0001$). Sunitinib treatment caused a 74% reduction in microvessel density ($p < 0.05$), an increase in tumor necrosis, and a decrease in number of GBM cells positive for MIB antibody. Sunitinib exhibited potent antiangiogenic activity that was associated with a meaningful prolongation of survival of mice bearing intracerebral GBM. These data support the potential utility of sunitinib in the treatment of GBM. *Neuro-Oncology 9, 412–423, 2007 (Posted to Neuro-Oncology [serial online], Doc. D06-00109, July 10, 2007. URL http://neuro-oncology.dukejournals.org; DOI: 10.1215/15228517-2007-024)*

Keywords: angiogenesis, antiangiogenic therapy, glioblastoma, invasion, sunitinib

Glioblastoma multiforme (GBM), the most frequent and aggressive type of primary brain tumor,[1] is associated with a high degree of vascularization.[2] This profuse angiogenesis, together with tumor cell dissemination in the brain,[3] is largely responsible for tumor recurrence and poor prognosis despite treatment. The median survival time for patients with GBM is about one year, emphasizing the need for development of novel therapeutic strategies for this challenging tumor. Depriving tumor cells of oxygen and nutrients by preventing angiogenesis appears to be a promising therapy for highly vascularized tumors such as GBM.[4,5]

Angiogenesis is characterized by a cascade of events that includes endothelial cell proliferation and migration, vessel sprouting, vascular permeability, and the remodeling of emerging vessels.[6] During tumorigenesis, an "angiogenic switch" is triggered by tumor expression

Received July 13, 2006; accepted January 4, 2007.

Address correspondence to Sophie de Boüard, GRECAN, Centre François Baclesse, Avenue du Général Harris, 14076 Caen, France (sophie.debouard@free.fr).

of various proangiogenic factors.[7] The production of proangiogenic factors is induced by physiological stimuli such as hypoxia, caused by increased tissue mass, and subsequent activation of hypoxia-inducible factor-1 (HIF-1).[8] Moreover, evidence suggests that genetic alterations in GBM cells lead to both an up-regulation of proangiogenic factors and a down-regulation of antiangiogenic factors, further tipping the balance in favor of angiogenesis and tumor progression.[8] Vascular endothelial growth factor (VEGF), the ligand for VEGF receptor (VEGFR), is the most potent of the myriad angiogenic factors described to date[9] and appears to play a major role in tumor- and hypoxia-induced angiogenesis in malignant glioma.[10] Its biological effects are elicited through two high-affinity receptor tyrosine kinases (RTKs), flt-1/VEGFR-1 and KDR/VEGFR-2, which are coexpressed on endothelial cells.[10] VEGF is up-regulated in GBM cells, and its main receptor, VEGFR-2, is expressed in the vascular endothelia of GBM.[11–13]

Increased expression of platelet-derived growth factor (PDGF) and PDGF receptor (PDGFR), frequently observed in malignant gliomas,[14–16] has also been implicated in GBM angiogenesis. Although glioma cells express PDGF ligands A and B and PDGFR-α, PDGFR-β is expressed only on tumor vasculature, particularly in the hyperplastic endothelium of GBM.[15,16] PDGF ligands enhance angiogenesis, at least in part, by stimulating VEGF expression in tumor endothelium expressing PDGFR-β[17] and by recruiting pericytes to neovessels.[18] These observations suggest both autocrine and paracrine actions of PDGF in tumor and particularly glioma angiogenesis. Moreover, the establishment of an autocrine loop attributable to the coexpression of PDGF and PDGFR also plays a role in GBM growth.[19,20] Thus, the biological effects mediated either directly or indirectly by the VEGFR and PDGFR RTKs are implicated in GBM angiogenesis. Preclinical studies indicate that dual inhibition of PDGFRs and VEGFRs produces robust antiangiogenic effects that may be superior to single-target inhibition.[21–23] Hence, inhibiting these targets in concert might be expected to result in broad antitumor efficacy.

Sunitinib malate (Sutent, SU11248) is a small, orally bioavailable molecule that has been identified as a low-nanomolar inhibitor of the angiogenic RTKs PDGFR-α and PDGFR-β, as well as VEGFR-1 and -2, KIT (stem cell factor receptor), and FLT3 (Fms-like tyrosine kinase-3 receptor).[24] This multitargeted RTK inhibitor has demonstrated broad and potent antiangiogenic and/or antitumor activity in preclinical studies, including tumor regression in murine models of human epidermal (A431), colon (Colo205 and HT-29), lung (NCI-H226 and H460), breast (MDA-MB-435), prostate (PC3-3M-luc), and renal (786-O) cancers, and suppression or delay in growth of many other tumor models, including subcutaneous C6, GL261, and SF763T glioma xenografts.[25,26] More recently, sunitinib has demonstrated efficacy with acceptable tolerability in a phase III clinical trial involving patients with gastrointestinal stromal tumor and two phase II trials involving patients with metastatic renal cell carcinoma,[24,27,28] and it is undergoing earlier stage clinical trials for various other cancers, including breast and non-small-cell lung tumors.[24] Promising sunitinib clinical results to date support the hypothesis that targeting VEGF- and PDGFR-mediated signaling is an effective approach in the treatment of human cancers.

With respect to GBM, to date sunitinib has been studied only in subcutaneous GBM models.[25,26] Therefore, it is unknown whether sunitinib is also effective in treating GBM grown in an orthotopic microenvironment, and whether it can improve survival in animals with intracerebrally growing GBM tumors. One aim of the present study was to investigate the antitumor and anti-invasive activities and potential survival benefits of sunitinib using orthotopic experimental models of human GBM in vitro and in vivo.

Materials and Methods

Drugs

Sunitinib (Pfizer Inc., New York, NY, USA) was suspended in dimethyl sulfoxide (DMSO) for in vitro studies and in carboxymethylcellulose (CMC) solution (CMC 0.5%, NaCl 1.8%, Tween 80 0.4%, and benzyl alcohol 0.9% in distillated water) for in vivo experiments (all solvents from Sigma, Saint-Quentin, France).

Cell Lines and Human Tumor Samples

The two human GBM cell lines used in the study, GL15 and U87MG, were cultured as previously described.[29] In addition, we used six fresh human specimens obtained from malignant glioma resection. After surgery, samples were immediately transferred to glioma-cell medium and prepared for implantation into brain slices obtained from young mice (see below). These tumors were classified according to the WHO 2000 classification.

Cell Count

GL15 and U87MG cells were plated in six-well plates at a density of 5×10^5 cells/well. After two days, cells were treated with DMSO alone or 100 nM, 1 μM, or 10 μM of sunitinib in DMSO. Each assay was performed in triplicate. One, two, three, four, and five days after treatment, cells were trypsinized, centrifuged at 300*g* for 6 min, and resuspended in 1 ml of phosphate-buffered saline (PBS). Viable cells were counted using Vi-cell (Beckman Coulter, Villepinte, France). Two independent experiments were performed.

Flow Cytometric Analysis

After treatment (see above), detached GL15 cells were collected separately, and adherent cells were dissociated using trypsin/EDTA. Adherent and detached cells were then pooled and centrifuged at 1,500*g* for 5 min before being fixed in 70% ethanol. Cells were centrifuged at 4,000*g* for 5 min and incubated for 30 min at

37°C in PBS. After centrifugation at 4,000*g* for 5 min, the cell pellets were resuspended at a final concentration of 10^6 cells/ml and stained with propidium iodide using the DNA Prep Coulter Reagent Kit (Beckman Coulter). Samples were analyzed at 15 mW using an EPICS XL flow cytometer (Beckman Coulter) equipped with a 488-nm argon laser. EXPO 32 Acquisition Software (Beckman Coulter) was used for data acquisition. Two independent experiments were performed.

Immunoprecipitation and Western Blot Analysis

GL15 and U87MG cells were treated with sunitinib (100 nM, 1 μM, or 10 μM) in DMSO or DMSO alone for 2 h. Two independent experiments were performed. After treatment, detached GL15 and U87MG cells were collected and adherent cells were dissociated using trypsin/EDTA. Adherent and detached cells were then pooled, centrifuged at 1,500*g* for 5 min, and lysed as previously described.[29] Protein concentrations were determined using the Bradford assay (Bio-Rad, Hercules, CA, USA).

Total phosphotyrosine-containing protein was immunoprecipitated from cell lysates (4G10 antibody; Upstate, Mundolsheim, France), and the amount of phosphorylated PDGFR-β and epidermal growth factor receptor (EGFR) in each sample was determined by Western blot analysis. The amount of total PDGFR-β and EGFR in each sample was determined by Western blot analysis without immunoprecipitation. Src and focal adhesion kinase (FAK) phosphorylation were studied by Western blot analysis without immunoprecipitation. Proteins were separated on a 4%–12% polyacrylamide gel (NuPAGE Novex 4%–12% Bis-Tris Gel; Invitrogen, Cergy Pontoise, France) and electrophoretically transferred onto a polyvinyl difluoride membrane (Millipore, Saint-Quentin-en-Yvelines, France). Membranes were blocked for 1 h at room temperature in Tween–Tris-buffered saline (T-TBS; 132 mM NaCl, 20 mM Tris-HCl pH 7.6, 0.5% Tween 20) supplemented with 5% nonfat dry milk and immunoblotted overnight at 4°C in T-TBS–milk 5% with the following primary antibodies: anti-PDGFR (1:1,000; Upstate), anti-EGFR (1:500; Santa Cruz, Le Perray en Yvelines, France), anti-pY418–Src (1:1,000; Biosource, Cliniscience, Montrouge, France), anti-Src (1:50; Oncogene Research, La Jolla, CA, USA), anti-pY397–FAK (1:1,000; Biosource), anti-FAK (1:1,000; Upstate), and anti–α-tubulin (1:3,000; Sigma). After three washes with T-TBS, the membrane was incubated for 1 h at room temperature in T-TBS–milk with the appropriate peroxidase-conjugated secondary antibody (antirabbit or antimouse immunglobulin G; Amersham, Orsay, France). After three washes with T-TBS, immunoreactivity was detected by enhanced chemiluminescence (ECL kit, Amersham). The extent of phosphorylation in sunitinib-treated cells was compared with that of untreated cells based on blot densitometry analysis using Scion Images software (Scion Corporation, Frederick, MD, USA).

Invasion Spheroid Assay

On reaching confluence, GBM cells were trypsinized, centrifuged at 300*g* for 10 min, and resuspended in 1 ml of glioma-cell medium. To obtain GL15 and U87MG spheroids, 5×10^5 cells were seeded in 1.5% agar-coated flasks for 7–10 days. Glioma-cell medium containing 100 nM, 1 μM, 5 μM, or 10 μM sunitinib in DMSO or DMSO alone was added to spheroids cultured in Matrigel (BD Biosciences, Le Pont de Claix, France). Tumor cell invasion was evaluated 24, 48, and 72 h after a single treatment with sunitinib or DMSO as described above (n = 13–24 spheroids in each group).

Organotypic Brain Slice Cultures

The organotypic assay was carried out as described previously,[30,31] using brain slices obtained from C57/BL6 mice (Charles River, Lyon, France) on postnatal day 6. GL15 or U87MG cells (5×10^3 in 0.1 μl) were injected into the cortex of brain slices 24 h after brain slice preparation using a 0.5-μl Hamilton syringe fixed on the arm of a micromanipulator (Narashige Inc., Tokyo, Japan). For freshly biopsied specimens, small fragments were deposited onto the slice surface and gently pushed with the tip of a needle until the tumor tissue was well enveloped by the parenchyma of the slice. Media containing 1 nM, 10 nM, 100 nM, 1 μM, or 10 μM sunitinib in DMSO or DMSO alone were changed three times per week (first medium change two days after slice preparation). Cultures were maintained for eight days and then fixed in 4% paraformaldehyde (PFA) at 4°C for 4 h. Tumor invasion and angiogenesis were evaluated at day 8 on 10–47 slices in each control or treated group, as described below. At least two independent experiments were performed.

Mouse Intracerebral Xenograft Models

The in vivo efficacy of sunitinib was studied in intracerebral xenograft models using the GL15 cell line for invasion[32] and the U87MG cell line for angiogenesis, tumor growth, and survival. Only GL15 cells exhibited high invasive capacities in the mouse brain;[32] in this context, this cell line was used to evaluate the effect of sunitinib on GBM invasion in vivo. Athymic mice (Charles River) received sterile rodent chow and water ad libitum. Treated mice were monitored twice daily. GL15 and U87MG cells were implanted into the striatum of the mice (2×10^5 cells in 2 μl), as previously described.[29] Animals were treated by oral administration of sunitinib in a CMC solution four days after stereotaxic glioma cell implantations. Mice bearing GL15 tumors were treated daily with an 80-mg/kg dose of sunitinib and sacrificed 25 days after implantation for postmortem analysis of glioma invasion, growth, and angiogenesis (n = 5 in each sample). Mice bearing U87MG tumors were treated with sunitinib 80 mg/kg per day using a five-day-on/two-day-off treatment cycle (5/2 schedule), or 80 mg/kg per day without treatment breaks (continuous administration). These animals were then either

maintained until death for determination of Kaplan-Meyer survival curves (n = 9 or 10 in each sample) or sacrificed 22 days after implantation and perfused for postmortem analysis of glioma invasion, growth, and angiogenesis (n = 3 in each sample). Survival analysis was performed in two independent experiments. Brains were sectioned serially on a cryostat at 20 μm thickness, and immunohistochemistry was performed as described below. The brains of dead mice were studied using histochemical and immunohistochemical analysis of formalin-fixed, paraffin-embedded 5-μm-thick sections.

Immunohistochemistry

Immunohistochemical analyses were carried out on cells, slice cultures, and selected sections from in vivo experiments following fixation with 4% PFA in PBS at 4°C (30 min for cell cultures, 4 h for brain slices) or in vivo after intracardiac perfusion as previously described.[29] Samples were incubated overnight at 4°C with monoclonal antibodies against human vimentin (1:400; Neo Markers; Interchim, Montluçon, France) and FAK (1:100; Upstate) or polyclonal antibodies against von Willebrand factor (factor VIII; 1:200; Dako, Glostrup, Denmark) and laminin (1:400; Sigma). Human vimentin antibody, used to detect GBM cells, does not cross-react with mouse antigen. After three washes in PBS, samples were incubated with a PBS solution containing antirabbit or antimouse immunoglobulin conjugated to cyamidine-Cy3 (1:500; Jackson Immuno Research, West Grove, PA, USA). The slices were mounted in Vectashield-containing DAPI. Some selected sections from in vivo experiments were incubated with anti–Ki-67 (MIB-1 antibody; 1:50; Immunotech, Marseilles, France) for quantification of proliferation in situ. Bound primary antibodies were detected using a Vector Elite ABC kit (Vector Laboratories, Burlingame, CA, USA) following the manufacturer's instructions and with diaminobenzidine as chromogen. Cell nuclei were counterstained with Mayer hematoxylin. In addition, Perl's staining with Kernechtrot counterstain was used to identify hemorrhages.

Quantification of Tumor Growth Parameters

Fluorescent microscopy (Olympus microscope BX51 equipped with a DP70 CCD camera) and fully automatic image processing routines (based on Aphelion software; ADCIS, Herouville Saint-Clair, France) were used to quantify tumor invasion and angiogenesis. Gray-level images of systematically sampled microscopic fields (n = 5) containing tumor vessels, immunostained for von Willebrand factor (in vitro) or laminin (in vivo), were collected at a magnification of 20× and a resolution of 0.78 μm. A fully automatic image processing routine was developed to measure the blood vessel density (μm^2 laminin per 10^5-μm^2 tumor), the total area of vessels, and the blood vessel length (μm^2 by optical field). The first two measures were obtained after a three-step segmentation procedure (3 × 3 modal filtering, mathematical morphology top hat transform using a 5 × 5 square structuring element and seeded region growing, 20 gray levels high). The blood vessel length was estimated as the area of the vessel after applying a skeleton operator followed by a four-connected pruning. A single gray-level image was collected at a magnification of 4× and a resolution of 3.10 μm to evaluate two invasion parameters: the tumor invasion area and the maximal distance of invasion. The tumor invasion area was defined as the ratio (A–A0)/A0, where A is the maximum area containing migrating glioma cells and A0 is the initial tumoral mass area; this ratio compensates for the heterogeneous sizes of implanted tumors, spheroids, and tumor fragments. The tumor invasion area of control tumors was considered as 100% of invasion; results are expressed as relative tumor invasion area (%). In addition, the maximal distance of invasion was assessed by the 80th percentile (P80) calculated from the distribution of all invasive cells. Then, P80 of each tumor was calculated in arbitrary units. The image processing algorithms used were similar to the method previously described to analyze blood vessel sprouting in an aortic ring model.[33] Briefly, the maximum distance of invasion was automatically estimated using successive mathematical morphology dilations of the initial tumor mass (20 × 20 square structuring element corresponding to 127.1 × 127.1 μm) and intersections with the binary image of the migrating glioma cells. To measure tumor volumes in vivo, we applied Cavalieri's principle on systematically sampled equidistant coronal sections.[34]

Statistical Analysis

Data in the text are presented as mean ± SEM. Mann-Whitney tests were used to compare groups of two. For analysis of differences between more than two groups, the post hoc unpaired Bonferroni t-test was used following a one-way analysis of variance. Survival data are presented as Kaplan-Meyer survival curves, using logrank analysis to determine statistical significance. The overall level of significance was set at 0.05 for all comparisons.

Results

Antiangiogenic Activity of Sunitinib in Organotypic Brain Slice Cultures

The in vitro activity of sunitinib on GL15 angiogenesis was evaluated using the organotypic brain slice model.[29] Modifications of the vascular network of the slice were observed around tumors in cultured brain slices treated with DMSO alone, with an increase of blood vessel density and a conspicuous preferential orientation of capillaries toward the implanted tumor. In contrast, a potent antiangiogenic effect was observed in human GBM tumors implanted in brain slices and treated with doses of sunitinib as low as 10 nM. Compared with control tumors, microvessel density (MVD) was reduced by 44% with 10 nM sunitinib and by 100% with sunitinib

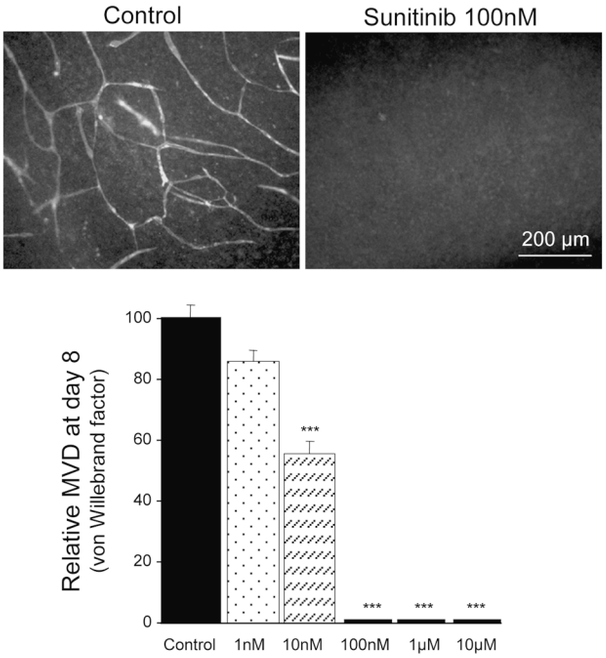

Fig. 1. Sunitinib inhibited tumor-related angiogenesis in mouse brain slices implanted with GL15 glioblastoma multiforme cells, as illustrated by representative photomicrographs of tumor vasculature (von Willebrand factor immunostaining) from untreated (left) and sunitinib-treated (right) slices bearing GL15 tumors. The bar graph shows the mean microvessel density percent change + SEM for sunitinib-treated slices compared with untreated control slices. The microvessel density was quantified at eight days. Scale bar = 200 µm. ***$p < 0.001$.

concentrations of 100 nM or greater ($p < 0.001$ for sunitinib- vs. vehicle-treated tumors; Fig. 1). Moreover, sunitinib treatment induced a decrease of already existing blood vessels in brain slice tissue. These observations suggest that sunitinib exhibited antiangiogenic activity against both developing and established vasculature in the brain slice model.

Sunitinib Induces Direct Antitumor Effects on GL15 Cells

To determine whether sunitinib induces direct cytostatic or cytotoxic effects on GBM cells, sunitinib (100 nM to 10 µM) was added to monolayer GL15 cultures, and cell cycle distribution and viability were monitored. At high concentration (10 µM), sunitinib inhibited GL15 cell growth by inducing G2/M growth arrest 24 h after a single treatment (Fig. 2A). In addition, 72 h after treatment with 10 µM sunitinib, about 40% of GL15 cell were apoptotic (Fig. 2A). Sunitinib enhancement of GBM cell apoptosis was further demonstrated by DAPI staining and caspase-3 cleavage 24 and 48 h after exposure to a single 10-µM dose of the drug (Fig. 2B).

Sunitinib Treatment Reduces GL15 Cell Invasion In Vitro and Decreases Src and FAK Phosphorylation at High Concentration

Because sunitinib is a multitargeted tyrosine kinase inhibitor, we also evaluated its effect on GBM cell invasion by inhibiting phosphorylation of kinases implicated in regulation of cell migration process.[25] To determine whether sunitinib reduces GBM invasion in vitro, GL15 and U87MG spheroids in Matrigel were treated with 100 nM, 1 µM, 5 µM, or 10 µM of sunitinib or DMSO alone. Tumor invasion parameters (relative tumor invasion area and maximal distance of cell invasion) were quantified 72 h after single-dose treatment. Sunitinib treatment caused a decrease in tumor invasion of GL15 and U87MG spheroids in Matrigel, as demonstrated by 36% and 46% ($p < 0.01$) reductions in the maximal distance of cell invasion, respectively, with 5 µM sunitinib and by 69% and 73% ($p < 0.001$) with 10 µM sunitinib. In addition, the 10-µM dose reduced the relative tumor invasion area of GL15 spheroids by 28% ($p < 0.01$) and of U87MG spheroids by 87% ($p < 0.001$).

To determine whether sunitinib is also effective in reducing GBM invasion in an orthotopic environment, GL15 cells were implanted into brain slice cultures and allowed to grow for eight days with DMSO vehicle or 100 nM, 1 µM, or 10 µM sunitinib before tumor invasion analysis. Sunitinib treatment resulted in a decrease in invasion by GL15 cells, as demonstrated by 18% ($p < 0.01$) and 42% ($p < 0.001$) reductions in maximal distances of cell invasion with the 1-µM and 10-µM doses, respectively (Fig. 3A). At 10 µM, sunitinib inhibited relative tumor invasion area by 49% ($p < 0.001$).

In experiments examining kinase phosphorylation in sunitinib- or vehicle-treated GL15 cells, inhibition of GBM invasion with high-dose sunitinib (10 µM) was associated with a decrease of Src Tyr418 (35%) and FAK Tyr397 (44%) phosphorylation 2 h after sunitinib treatment (Fig. 3B), whereas EGFR kinase was not inhibited at this concentration. We did not observe any apoptotic effects 2 h after sunitinib treatment. Treated cells also exhibited extensive morphological changes and a decrease of focal adhesion staining (Fig. 3C). Because of the dramatic difference in sunitinib concentration required to completely inhibit angiogenesis and PDGFR-β phosphorylation (100 nM) compared with cell invasion (5–10 µM) in vitro, the relevance of this finding is uncertain.

Antitumor Activities of Sunitinib on Fresh Human Malignant Gliomas in Brain Slice Cultures

The antiangiogenic and anti-invasive effects of high-dose sunitinib (10 µM) obtained with GBM cell lines were confirmed using fragments of six fresh human glioma biopsy specimens implanted into brain slice cultures. These tumors were classified as GBMs in three cases, anaplastic astrocytoma grade III in two, and oligoastrocytoma grade III in one, using the WHO 2000 classification. We observed a total inhibition of angiogenesis in all human gliomas tested and a reduction of

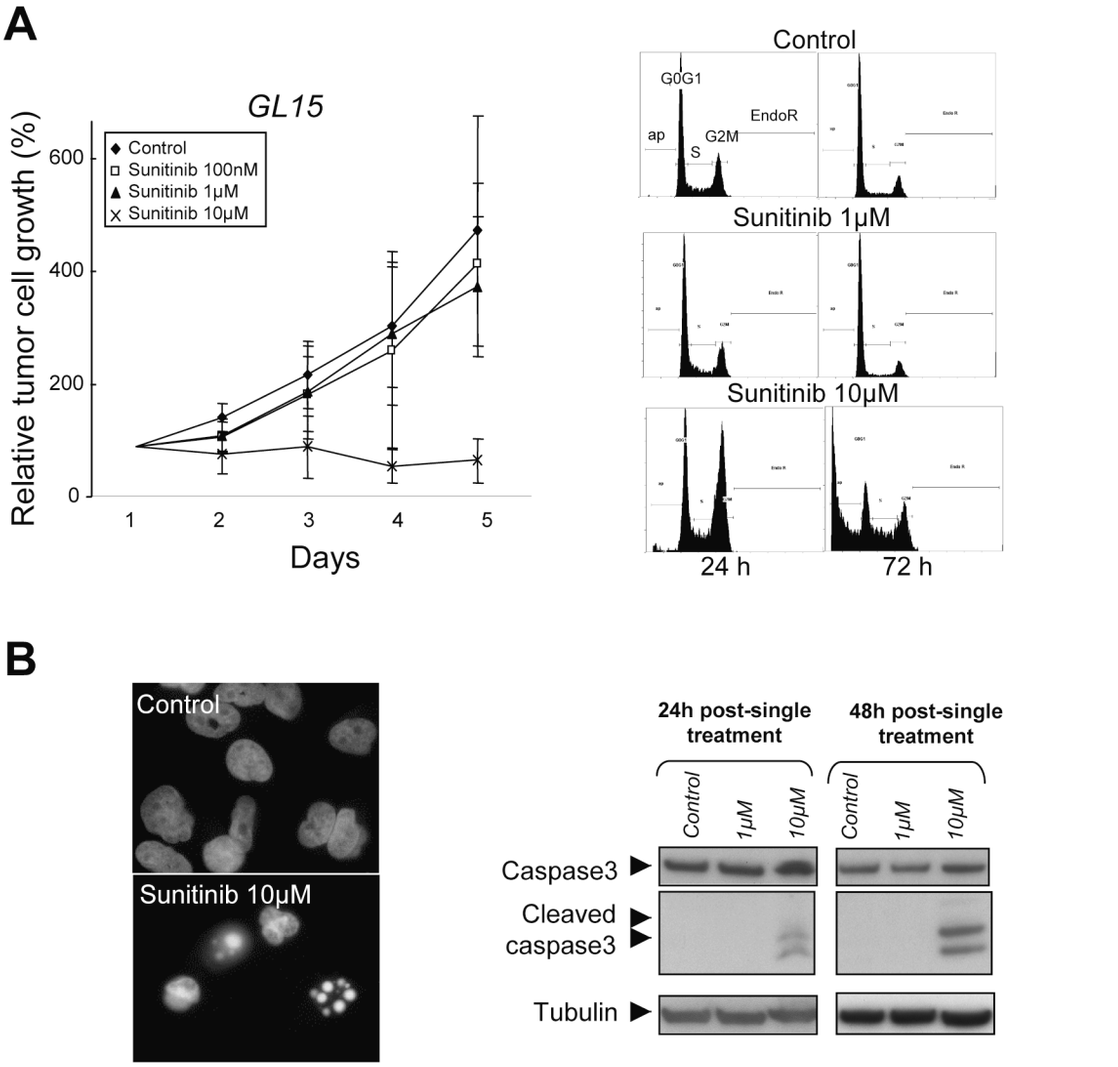

Fig. 2. (A) Direct antitumor effects of sunitinib (100 nM to 10 μM) on GL15 cells were evaluated using cell count (1–5 days) and flow cytometry analysis (24 and 72 h). High-dose sunitinib (10 μM) produced direct antitumor effects after a single-dose exposure. Abbreviations: ap, apoptosis; Endo R, endoreplication. (B) Treatment with high-dose sunitinib also induced GL15 apoptosis, as demonstrated by DAPI staining and caspase-3 cleavage, 24 and 48 h after single-dose exposure.

cell invasion by 38%–75% in four of six gliomas (Fig. 4). These results suggest that the antiangiogenic activity of sunitinib is mediated through its action on neovascular endothelial cells, independent of the tumor type.

Sunitinib Does Not Reduce GL15 Cell Invasion in the Mouse Intracerebral Model

In order to determine whether sunitinib is potent enough to reduce cell invasion in vivo, the highly invasive GL15 cells were implanted into the striatum of athymic mice and allowed to grow for four days prior to initiating sunitinib treatment. Athymic mice bearing GL15 tumors were orally administered sunitinib at 80 mg/kg per day and sacrificed 25 days after tumor cell implantation for postmortem analysis of GBM invasion. Despite use of the maximum tolerated dose, there was no evidence of a direct anti-invasive effect (invasion area: $1.18 \pm 0.16 \times 10^6$ for control vs. $1.51 \pm 0.09 \times 10^6$ μm^2 for treated mice, $p = 0.45$).

Antiangiogenic Efficacy of Sunitinib in a Mouse Model of Intracerebral GBM

The antiangiogenic activity of sunitinib in vivo was studied using the intracerebral U87MG xenograft model. Athymic mice bearing four-day-old U87MG tumors received oral treatment with 80 mg/kg sunitinib (schedule 5/2), in order to mimic the human schedule, and were sacrificed 22 days after implantation for postmortem analysis of GBM angiogenesis and growth. At 22 days, a dense network of blood vessels was observed

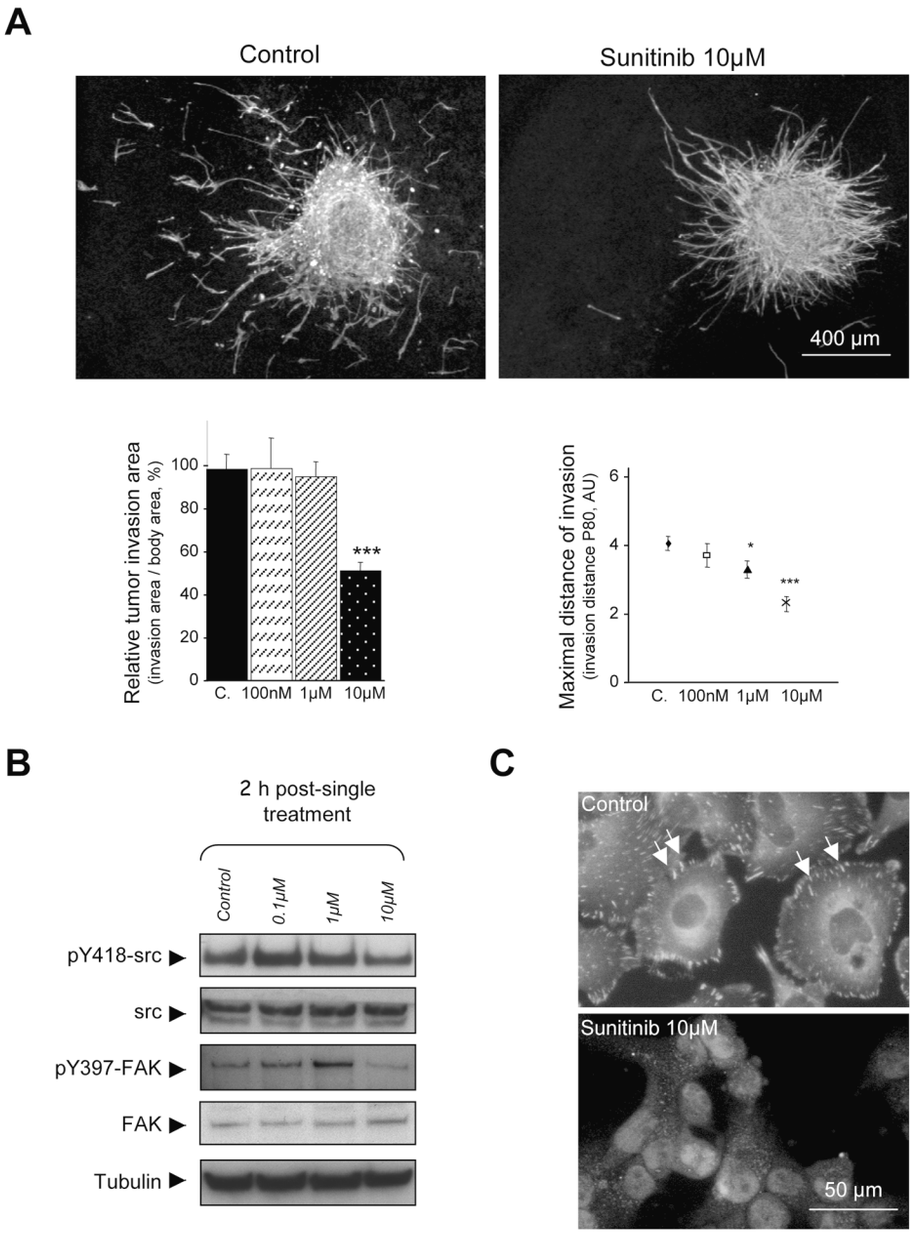

Fig. 3. (A) Representative photomicrographs of GL15 tumors from untreated (left) and sunitinib-treated (right) brain slices show that high-dose sunitinib (10 μM) decreased tumor invasion. Sunitinib treatment induced a dose-dependent decrease in tumor invasion, with a 49% reduction in relative tumor invasion area at 10 μM and with 18% and 42% reductions in maximal distance of cell invasion at 1 μM and 10 μM, respectively. Abbreviations: P80, 80th percentile; AU, arbitrary units; C, control. Scale bar = 400 μm. *$p < 0.05$; ***$p < 0.001$. (B) High-dose sunitinib treatment was associated with a 44% and 35% decrease in Src and focal adhesion kinase phosphorylation, respectively, as demonstrated by Western blot analysis. (C) Cells treated with a 10-μM dose of sunitinib exhibited extensive morphological changes that included decreases in focal adhesion staining (arrows). Scale bar = 50 μm.

in the control tumor mass and at its margin. In sharp contrast, the density of blood vessels was drastically reduced in tumors from sunitinib-treated mice (Fig. 5A). Sunitinib treatment produced a 74% reduction in tumor MVD (18,267 ± 1,244 vs. 4,702 ± 568 μm^2 per 10^5-μm^2 tumor, $p < 0.05$) and in average blood vessel length (18,105 ± 1,419 vs. 4,712 ± 599 μm by optical field, $p < 0.05$; Fig. 5A). As a consequence of vascular changes, volumes of tumors resected from treated mice were smaller than those from control mice. The control tumor volume was $3.8 \pm 1.4 \times 10^8$ versus $2 \pm 0.4 \times 10^8$ μm^3 for sunitinib-treated tumors.

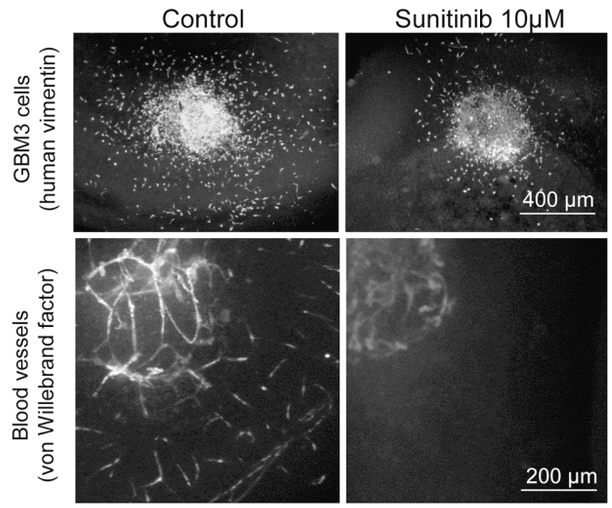

Tumor	Inhibition of invasion (Sunitinib 10μM)
GBM1	NS
GBM2	NS
GBM3	38.3%, $p < 0.05$
AA 1	54.9% $p < 0.001$
AA 2	74.4%, $p < 0.05$
AOA	60.8%, $p < 0.0001$

Fig. 4. The anti-invasive and antiangiogenic effects of high-dose sunitinib (10 μM) on tumor cells were confirmed using fragments of six fresh human malignant glioma specimens implanted into brain slice cultures. Representative photomicrographs of untreated (left) and sunitinib-treated (right) GBM3 show a decrease in GBM3 cell invasion (human vimentin staining; scale bar = 400 μm) and inhibition of angiogenesis (von Willebrand factor staining; scale bar = 200 μm). The table summarizes the anti-invasive effect of sunitinib on six different human malignant gliomas. Abbreviations: AA, anaplastic astrocytoma; AOA, anaplastic oligoastrocytoma.

In addition, the antitumor effects of sunitinib treatment were evaluated by histological and immunohistochemical analysis of tumors from treated and untreated animals. The absence of a regular network of vessels capable of bringing oxygen and nutrients to the treated tumor cells was associated with massive necrosis in the central portions of these tumors as well as areas of micronecrosis in the periphery of the tumor tissue (Fig. 5B). In contrast, necrotic areas were not observed in control tumors (Fig. 5B). Histological studies also showed that sunitinib treatment was associated with a decrease in MIB-1–positive U87MG cells, indicating a decrease in cell proliferation (Fig. 5B).

Effects of Sunitinib on Survival in Mice Bearing Intracerebral GBM Tumors

To determine whether sunitinib is sufficiently potent to prolong survival in animals with GBM tumors, athymic mice bearing intracerebral U87MG tumors were treated with 80 mg/kg per day sunitinib (5/2 schedule [discontinuous, as in humans] or continuous treatment protocol [maximal tolerated dose]) and maintained until death for Kaplan-Meyer analysis. Sunitinib administered using the 5/2 schedule enhanced mouse survival by 36% (median survival, 34 days vs. 25 days; $p = 0.0001$; Fig. 6). The continuous treatment schedule did not provide additional survival benefits (median survival, 27 days vs. 24 days; $p = 0.012$) compared with the discontinuous (5/2 schedule) treatment protocol. Sunitinib treatment was not curative in any mice in the present study. After two weeks of treatment, paralysis (hemiplegia contralateral to tumor) was observed in 4 of the 12 mice in the continuous treatment group, 1 of the 10 mice in the 5/2 schedule group, and 1 of the 10 mice in the control group. Postmortem analysis of symptomatic mice revealed large tumors with necrotic microhemorrhages. Positive Perl's staining allowing detection of heme deposits was observed in only one of the six autopsies, suggesting that microhemorrhages were late events. Microhemorrhages were not detected in the GL15 intracranial GBM model. Further studies in larger cohorts are warranted to evaluate the relevance of this finding and relationship to sunitinib administration schedule.

Discussion

Antiangiogenic therapy shows promise as a treatment strategy for highly vascularized tumors such as GBM.[2,4,5] Sunitinib is a multitargeted kinase inhibitor that selectively inhibits various RTKs, including those playing key roles in angiogenesis, such as VEGFRs and PDGFRs.[24] The present study evaluated the antiangiogenic and antitumor activities of sunitinib on experimental orthotopic GBM examined both in vitro and in vivo. The main finding of the present study is that oral sunitinib treatment results in a potent inhibition of angiogenesis, leading to a meaningful prolongation of survival of mice bearing intracerebral GBM.

Because sunitinib inhibits both VEGFRs and PDGFRs, it is expected to simultaneously target endothelial cells, pericytes, and GBM cells expressing PDGFR.[20] Thus, in addition to antiangiogenic effects, sunitinib should be able to exert direct antitumor activity against glioma cells that rely on PDGFR for proliferation and survival. In this context, the present study examined the effects of sunitinib treatment on PDGFR-expressing GBM cells in vitro and showed that antiproliferative and proapoptotic effects were limited to high-dose (10 μM) sunitinib. This sunitinib concentration did not exhibit any toxic effects on fetal rat astrocytes or neurons in primary cultures (data not shown).

Interestingly, sunitinib treatment also produced an anti-invasive effect on GBM cells in the two in vitro experimental models used: GBM spheroids in Matrigel and GBM cells in brain slice cultures. We explored whether this effect of sunitinib might be mediated, at least in part, through inhibition of kinases implicated in regulation of GBM cell migration processes, such as FAK and Src.[35–37] Mendel et al.[25] have shown that suni-

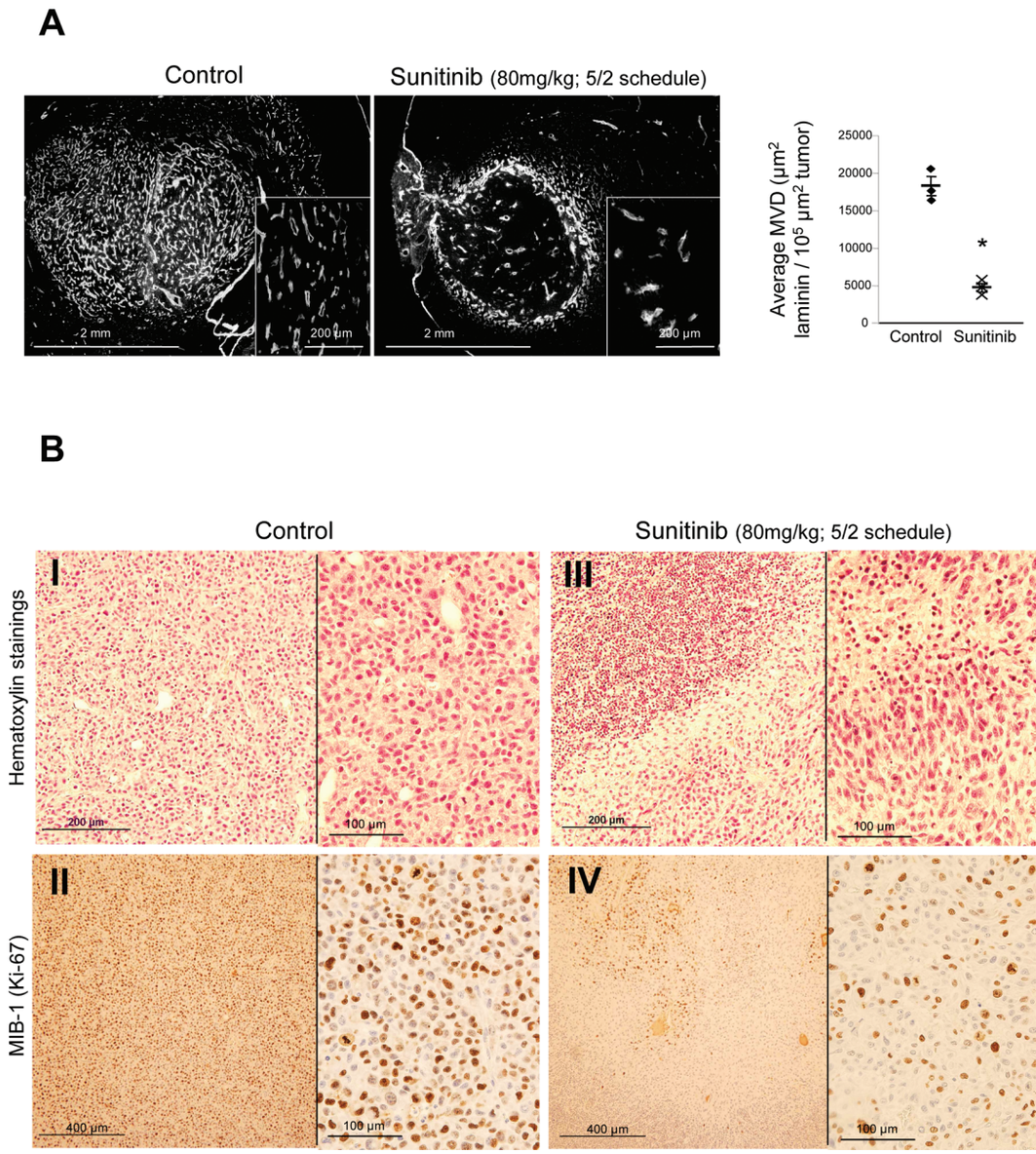

Fig. 5. Sunitinib reduces angiogenesis of intracranial U87MG tumors. Athymic mice bearing U87MG tumors were treated with an 80 mg/kg per day dose of sunitinib (schedule 5/2) and sacrificed 22 days after implantation. Brain sections 20 μm thick were subjected to von Willebrand factor immunohistochemistry and hematoxylin staining. (A) Representative photomicrographs from U87MG untreated (left) and sunitinib-treated (right) tumors, and accompanying graphs, show that sunitinib treatment produced 74% reductions in tumor microvessel density (18,267 ± 1,244 μm^2 vs. 4,702 ± 568 μm^2 per 10^5-μm^2 tumor; $p < 0.05$). (B) Hematoxylin staining of sections shows that sunitinib treatment was associated with tumor necrosis (panel I vs. III) and decreases in U87MG proliferation, as demonstrated by reduced MIB-1 (Ki-67) immunostaining (panel II vs. IV).

tinib competes with ATP for binding in the ATP-binding pocket of Src (half-maximal inhibitory concentration [IC_{50}] = 0.6 μM). In our experimental conditions, the anti-invasive activity of sunitinib was associated with partial inhibition of Src Tyr418 and FAK Tyr397 phosphorylation 2 h after administration of a single dose of sunitinib to GBM cells. Interestingly, another recent study demonstrated up-regulation of cadherin-11 in xenograft tumors (including subcutaneous C6 rat glioma) and in some human tumor biopsies in response to sunitinib treatment in vivo.[38] Functionally, expression of wild-type cadherin-11 increases the adhesive nature and decreases the invasive capacity of various tumor cells.[39,40] Therefore, sunitinib-induced up-regulation of cadherin-11 levels might alter the adhesive nature of treated tumor cells. The mechanism by which sunitinib

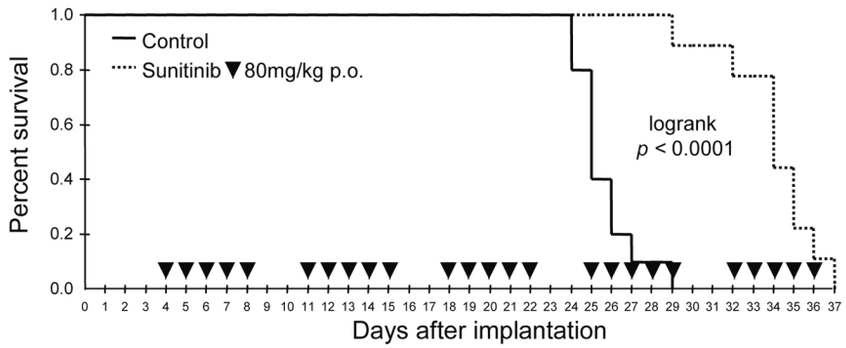

Fig. 6. Orally administered sunitinib increased survival of mice bearing intracranial U87MG glioma. Analysis of Kaplan-Meyer survival curves ($n = 10$ in each sample) showed that sunitinib 80 mg/kg per day (5/2 schedule) enhanced survival by 36% compared with control (median survival, 34 days vs. 25 days; $p < 0.0001$).

inhibition of angiogenic RTKs, Src, or FAK leads to increased expression of cadherin-11 is unknown.[38]

However, in relation to interpreting the relevance of effects observed in vitro at high concentrations of sunitinib, a concentration of 10 μM is likely to have an insufficient degree of potency based on the following pharmacological observations: (1) the minimum plasma concentration (sunitinib and its active metabolite) required to completely inhibit phosphorylation of critical sunitinib RTK targets in vivo is approximately 50–100 ng/ml (free plasma concentration of 2.5–5 ng/ml or 0.005–0.01 μM),[25] and (2) minimal evidence of inhibition of fibroblast growth factor receptor-1 (an RTK with an IC_{50} of 0.8 μM, which is 50- to 100-fold greater than that of intended sunitinib RTK targets) was observed at plasma concentrations 10-fold higher than the minimum plasma concentration required to inhibit sunitinib RTK targets in tumors in vivo.[25] In addition, the median plasma levels observed in human studies (~0.1 μM) are 500- to 1,000-fold below plasma levels predicted to be required for pharmacologically relevant inhibition of kinase targets in the 10-μM range.[41] As a consequence, the anti-invasive activity of sunitinib observed in vitro was not similarly observed in vivo. Invasive capacities of GL15 cells in the sunitinib-treated brain were similar to those observed in the untreated brain. Alternatively, this failure of anti-invasive effect may be due to a parallel increase in glioma invasion during antiangiogenic therapy.[29,42,43] Instead, it has been recently suggested that antiangiogenic therapy, which increases tumor hypoxia, may increase cell invasion by activating proinvasive signaling pathways.[44]

The ability of sunitinib to exert antiangiogenic effects in an intracranial GBM model is a new and important finding. Previous studies demonstrating antiangiogenic effects of sunitinib on gliomas were restricted to subcutaneous GBM models.[25,26] The results of the present study indicate that sunitinib may exert important antiangiogenic and antitumor effects on GBM tumors growing in their natural environment. Of note, the survival experiments demonstrated that the antiangiogenic effects of sunitinib in this intracranial GBM model were associated with significant prolongation of survival. This suggests that the antiangiogenic effects of sunitinib may translate into improved outcomes for mice bearing these intracranial tumors, although the results have also shown that a sunitinib monotherapy fails to cure animals.

A comparison of continuous versus discontinuous (5/2 schedule) administration of 80 mg/kg sunitinib to mice bearing intracranial U87MG tumors showed that the continuous treatment regimen was associated with a higher incidence of side effects. For example, hemiplegia contralateral to tumor appeared in 33% of mice in the continuous treatment group after at least two weeks of sunitinib treatment, compared with an incidence rate of only 10% in the discontinuous sunitinib and control groups. Postmortem analysis of symptomatic mice revealed large tumors with necrotic microhemorrhages. Of interest, hemorrhages were not found in the GL15 intracranial GBM model or in other experimental studies using sunitinib,[25,26] suggesting that symptomatic hemorrhages may be related to the U87MG experimental model. However, we could not exclude the possibility that hemorrhages may also be related to the high and continuous dose of sunitinib. The acute and rapid destabilization of blood vessels and necrosis of tumors deprived of oxygen provide the basis for intratumoral hemorrhages. Bleeding (including minor mucocutaneous hemorrhage, major hemoptysis, and tumor hemorrhage) is the most prominent adverse effect observed in clinical trials with other antiangiogenic drugs[45] and may explain intratumoral hemorrhage observed with the continuous treatment protocol used in the present study. Clearly, bleeding event is an important caveat to using antiangiogenic inhibitors in treating patients with large brain tumors, especially when this treatment is associated with radiation therapy, which already leads to transient vessel destabilization per se. However, it is worth noting that the continuous dosing regimen used in this study is quite different from the discontinuous dosing regimen of sunitinib that has been used in cancer patients (50 mg/day administered in cycles of four weeks on, two weeks off treatment) and that has been shown to produce effi-

cacy with manageable toxicity.[27] Given the fact that high dosage and continuous regimen did not result in a better efficacy, we suggest that lower dose and discontinuous regimen should be used in future clinical trials. Moreover, intratumoral hemorrhage should be closely monitored with radiological imagery.

Taken together, these findings suggest that sunitinib may have utility in clinical applications, such as preventing tumor recurrence after surgery, in association with radiotherapy and chemotherapy. Further evaluation of sunitinib dosing regimens, of conditions that are associated with microhemorrhages, and of combined treatment with alkylating drugs are warranted.

Acknowledgments

This work was supported by La Ligue contre le cancer (National Committee and Calvados Committee; S.D.B.), l'Association pour la Recherche sur le Cancer (ARC-7813), and Le Conseil Régional de Basse Normandie. We thank Jean-Michel Derlon for providing fresh tumor specimens. We thank Maryline Duval, Olivier Nicole, and Christian Lebeau for technical support on flow cytometry analysis, neuronal toxicity studies, and MIB-1 immunohistochemistry, respectively. We thank Marie-Christine Bon and Marie-Hélène Louis for technical support in the animal house.

References

1. Kleihues P, Burger PC, Collins VP, Newcomb EW, Oghaki H, Cavanee WK. Glioblastoma. In: Kleihues P, Cavanee WK, eds. *Tumours of the Nervous System: Pathology and Genetics*. Lyon, France: International Agency for Research on Cancer Press; 2000;29–98.
2. Plate KH, Risau W. Angiogenesis in malignant gliomas. *Glia*. 1995; 15:339–347.
3. Bernstein JJ. Local invasion and intraparenchymal metastasis of astrocytomas. *Neuropathol Appl Neurobiol*. 1996;22:421–424.
4. Ferrara N, Kerbel RS. Angiogenesis as a therapeutic target. *Nature*. 2005;438:967–974.
5. Puduvalli VK. Inhibition of angiogenesis as a therapeutic strategy against brain tumors. *Cancer Treat Res*. 2004;117:307–336.
6. Carmeliet P. Angiogenesis in life, disease and medicine. *Nature*. 2005;438:932–936.
7. Hanahan D, Folkman J. Patterns and emerging mechanisms of the angiogenic switch during tumorigenesis. *Cell*. 1996;86:353–364.
8. Kaur B, Tan C, Brat DJ, Post DE, Van Meir EG. Genetic and hypoxic regulation of angiogenesis in gliomas. *J Neurooncol*. 2004;70:229–243.
9. Ferrara N. VEGF and the quest for tumour angiogenesis factors. *Nat Rev Cancer*. 2002;2:795–803.
10. Ferrara N, Gerber HP, LeCouter J. The biology of VEGF and its receptors. *Nat Med*. 2003;9:669–676.
11. Plate KH, Breier G, Millauer B, Ullrich A, Risau W. Up-regulation of vascular endothelial growth factor and its cognate receptors in a rat glioma model of tumor angiogenesis. *Cancer Res*. 1993;53:5822–5827.
12. Samoto K, Ikezaki K, Ono M, et al. Expression of vascular endothelial growth factor and its possible relation with neovascularization in human brain tumors. *Cancer Res*. 1995;55:1189–1193.
13. Schmidt NO, Westphal M, Hagel C, et al. Levels of vascular endothelial growth factor, hepatocyte growth factor/scatter factor and basic fibroblast growth factor in human gliomas and their relation to angiogenesis. *Int J Cancer*. 1999;19:10–18.
14. Guha A, Dashner K, Black PM, Wagner JA, Stiles CD. Expression of PDGF and PDGF receptors in human astrocytoma operation specimens supports the existence of an autocrine loop. *Int J Cancer*. 1995;60:168–173.
15. Hermanson M, Funa K, Hartman M, et al. Platelet-derived growth factor and its receptors in human glioma tissue: expression of messenger RNA and protein suggests the presence of autocrine and paracrine loops. *Cancer Res*. 1992;52:3213–3219.
16. Plate KH, Breier G, Farrell CL, Risau W. Platelet-derived growth factor receptor-beta is induced during tumor development and upregulated during tumor progression in endothelial cells in human gliomas. *Lab Invest*. 1992;67:529–534.
17. Wang D, Huang HJ, Kazlauskas A, Cavenee WK. Induction of vascular endothelial growth factor expression in endothelial cells by platelet-derived growth factor through the activation of phosphatidylinositol 3-kinase. *Cancer Res*. 1999;59:1464–1472.
18. Guo P, Hu B, Gu W, et al. Platelet-derived growth factor-B enhances glioma angiogenesis by stimulating vascular endothelial growth factor expression in tumor endothelia and by promoting pericyte recruitment. *Am J Pathol*. 2003;162:1083–1093.
19. Lokker NA, Sullivan CM, Hollenbach SJ, Israel MA, Giese NA. Platelet-derived growth factor (PDGF) autocrine signaling regulates survival and mitogenic pathways in glioblastoma cells: evidence that the novel PDGF-C and PDGF-D ligands may play a role in the development of brain tumors. *Cancer Res*. 2002;62:3729–3735.
20. Westermark B, Heldin CH, Nister M. Platelet-derived growth factor in human glioma. *Glia*. 1995;15:257–263.
21. Bergers G, Song S, Meyer-Morse N, Bergsland E, Hanahan D. Benefits of targeting both pericytes and endothelial cells in the tumor vasculature with kinase inhibitors. *J Clin Invest*. 2003;111:1287–1295.
22. Erber R, Thurnher A, Katsen AD, et al. Combined inhibition of VEGF and PDGF signaling enforces tumor vessel regression by interfering with pericyte-mediated endothelial cell survival mechanisms. *FASEB J*. 2004;18:338–340.
23. Laird AD, Christensen JG, Li G, et al. SU6668 inhibits Flk-1/KDR and PDGFRbeta in vivo, resulting in rapid apoptosis of tumor vasculature and tumor regression in mice. *FASEB J*. 2002;16:681–690.
24. Sakamoto KM. Su-11248 Sugen. *Curr Opin Investig Drugs*. 2004;5: 1329–1339.
25. Mendel DB, Laird AD, Xin X, et al. In vivo antitumor activity of SU11248, a novel tyrosine kinase inhibitor targeting vascular endothelial growth factor and platelet-derived growth factor receptors: determination of a pharmacokinetic/pharmacodynamic relationship. *Clin Cancer Res*. 2003;9:327–337.
26. Schueneman AJ, Himmelfarb E, Geng L, et al. SU11248 maintenance therapy prevents tumor regrowth after fractionated irradiation of murine tumor models. *Cancer Res*. 2003;63:4009–4016.

27. Faivre S, Delbaldo C, Vera K, et al. Safety, pharmacokinetic, and antitumor activity of SU11248, a novel oral multitarget tyrosine kinase inhibitor, in patients with cancer. *J Clin Oncol*. 2006;24:25–35.
28. Motzer RJ, Michaelson MD, et al. Activity of SU11248, a multitargeted inhibitor of vascular endothelial growth factor receptor and platelet-derived growth factor receptor, in patients with metastatic renal cell carcinoma. *J Clin Oncol*. 2006;24:16–24.
29. de Boüard S, Guillamo JS, Christov C, et al. Antiangiogenic therapy against experimental glioblastoma using genetically engineered cells producing interferon-alpha, angiostatin, or endostatin. *Hum Gene Ther*. 2003;14:883–895.
30. de Boüard S, Christov C, Guillamo JS, et al. Invasion of human glioma biopsy specimens in cultures of rodent brain slices: a quantitative analysis. *J Neurosurg*. 2002;97:169–176.
31. Stoppini L, Buchs PA, Muller D. A simple method for organotypic cultures of nervous tissue. *J Neurosci Methods*. 1991;37:173–182.
32. Guillamo JS, Lisovoski F, Christov C, et al. Migration pathways of human glioblastoma cells xenografted into the immunosuppressed rat brain. *J Neurooncol*. 2001;52:205–215.
33. Gommes CJ, de Jong K, Pirard JP, Blacher S. Assessment of the 3D localization of metallic nanoparticles in Pd/SiO2 cogelled catalysts by electron tomography. *Langmuir*. 2005;20:12378–12385.
34. Howard CV, Reed MG. *Unbiased Stereology, Three-Dimensional Measurement in Microscopy*. Guildford, UK: BIOS Scientific Publishers; 1998.
35. Angers-Loustau A, Hering R, Werbowetski TE, Kaplan DR, Del Maestro RF. SRC regulates actin dynamics and invasion of malignant glial cells in three dimensions. *Mol Cancer Res*. 2004;2:595–605.
36. Jones G, Machado J Jr, Merlo A. Loss of focal adhesion kinase (FAK) inhibits epidermal growth factor receptor-dependent migration and induces aggregation of nh(2)-terminal FAK in the nuclei of apoptotic glioblastoma cells. *Cancer Res*. 2001;61:4978–4981.
37. Jones G, Machado J Jr, Tolnay M, Merlo A. PTEN-independent induction of caspase-mediated cell death and reduced invasion by the focal adhesion targeting domain (FAT) in human astrocytic brain tumors which highly express focal adhesion kinase (FAK). *Cancer Res*. 2001;61:5688–5691.
38. Morimoto AM, Tan N, West K, et al. Gene expression profiling of human colon xenograft tumors following treatment with SU11248, a multitargeted tyrosine kinase inhibitor. *Oncogene*. 2004;23:1618–1626.
39. Feltes CM, Kudo A, Blaschuk O, Byers SW. An alternatively spliced cadherin-11 enhances human breast cancer cell invasion. *Cancer Res*. 2002;62:6688–6697.
40. Kashima T, Nakamura K, Kawaguchi J, et al. Overexpression of cadherins suppresses pulmonary metastasis of osteosarcoma in vivo. *Int J Cancer*. 2003;20:147–154.
41. Motzer RJ, Hoosen S, Bello CL, Christensen JG. Sunitinib malate for the treatment of solid tumours: a review of current clinical data. *Expert Opin Investig Drugs*. 2006;15:553–561.
42. Kunkel P, Ulbricht U, Bohlen P, et al. Inhibition of glioma angiogenesis and growth in vivo by systemic treatment with a monoclonal antibody against vascular endothelial growth factor receptor-2. *Cancer Res*. 2001;61:6624–6628.
43. Rubenstein JL, Kim J, Ozawa T, et al. Anti-VEGF antibody treatment of glioblastoma prolongs survival but results in increased vascular cooption. *Neoplasia*. 2000;2:306–314.
44. Pennacchietti S, Michieli P, Galluzzo M, Mazzone M, Giordano S, Comoglio PM. Hypoxia promotes invasive growth by transcriptional activation of the met protooncogene. *Cancer Cell*. 2003;3:347–361.
45. Johnson DH, Fehrenbacher L, Novotny WF, et al. Randomized phase II trial comparing bevacizumab plus carboplatin and paclitaxel with carboplatin and paclitaxel alone in previously untreated locally advanced or metastatic non-small-cell lung cancer. *J Clin Oncol*. 2004;22:2184–2191.